Effects of ice-crystal structure on halo formation: cirrus cloud experimental and ray-tracing modeling studies

Kenneth Sassen, Nancy C. Knight, Yoshihide Takano, and Andrew J. Heymsfield

During the 1986 Project FIRE (First International Satellite Cloud Climatology Project Regional Experiment) field campaign, four 22° halo-producing cirrus clouds were studied jointly from a ground-based polarization lidar and an instrumented aircraft. The lidar data show the vertical cloud structure and the relative position of the aircraft, which collected a total of 84 slides by impaction, preserving the ice crystals for later microscopic examination. Although many particles were too fragile to survive impaction intact, a large fraction of the identifiable crystals were columns and radial bullet rosettes, with both displaying internal cavitations, and radial plate-column combinations. Particles that were solid or displayed only a slight amount of internal structure were relatively rare, which shows that the usual model postulated by halo theorists, i.e., the randomly oriented, solid hexagonal crystal, is inappropriate for typical cirrus clouds. With the aid of new ray-tracing simulations for hexagonal hollow-ended column and bullet-rosette models, we evaluate the effects of more realistic ice-crystal structures on halo formation and lidar depolarization and consider why the common halo is not more common in cirrus clouds.

1. Introduction

Halos are sometimes a spectacular feature associated with the ubiquitous cirrus clouds of the upper troposphere. Aside from the beauty of vividly colored halo displays, though, their geometries, when applied to models, have been useful in demonstrating the presence of light scatterers that display a fundamental hexagonal symmetry and a preference for certain fall orientations. Thus cirrus cloud optical phenomena are not only aesthetically pleasing, but these concentrations of scattered light in the phase functions of cirrus cloud particles have also made them important passive remote sensing tools. The broader information that describes the complete angular scattering properties of cirrus clouds is of considerable importance for simulating the effects of these high clouds in radiative transfer and climate research. However, because of their inaccessibility for *in situ* study, knowledge of the exact shapes of cirrus particles is far from satisfactory, such that the relatively simple hexagonal ice-crystal models that readily lend themselves to theoretical simulation and that successfully replicate halos may not yield angular scattering predictions appropriate for typical cirrus clouds.

What is currently known of the composition of cirrus clouds comes largely from aircraft studies that utilize various laser-based *in situ* size spectrometer probes that, although capable of acquiring vast amounts of data, do not yield detailed information on particle structure. The most commonly used two-dimensional ice-particle shadow probes, which display minimum particle resolutions of 25 to 100 μm, depending on aircraft velocity and particle type, can provide only limited data on ice-crystal shape and orientation. (This lower limit on detectable particle size has led to controversy over the radiative transfer impact of undetected cirrus particles.[1]) Furthermore, no information on the three-dimensional and internal structures of ice particles can be recovered. As explored here, it is just such information that is crucial to understanding the angular scattering behavior of cirrus clouds, especially with regard to halo formation.

Fortunately increasing effort is being directed toward the collection *in situ* of cirrus ice-crystal samples by impaction for later microscopic examination. These cloud samples can be preserved either temporarily or permanently by the collection of particles on

K. Sassen and Y. Takano are with the Department of Meteorology, University of Utah, Salt Lake City, Utah 84112; N. C. Knight and A. J. Heymsfield are with the National Center for Atmospheric Research, Boulder, Colorado 80303.

Received 27 September 1993; revised manuscript received 10 January 1994.

0003-6935/94/214590-12$06.00/0.

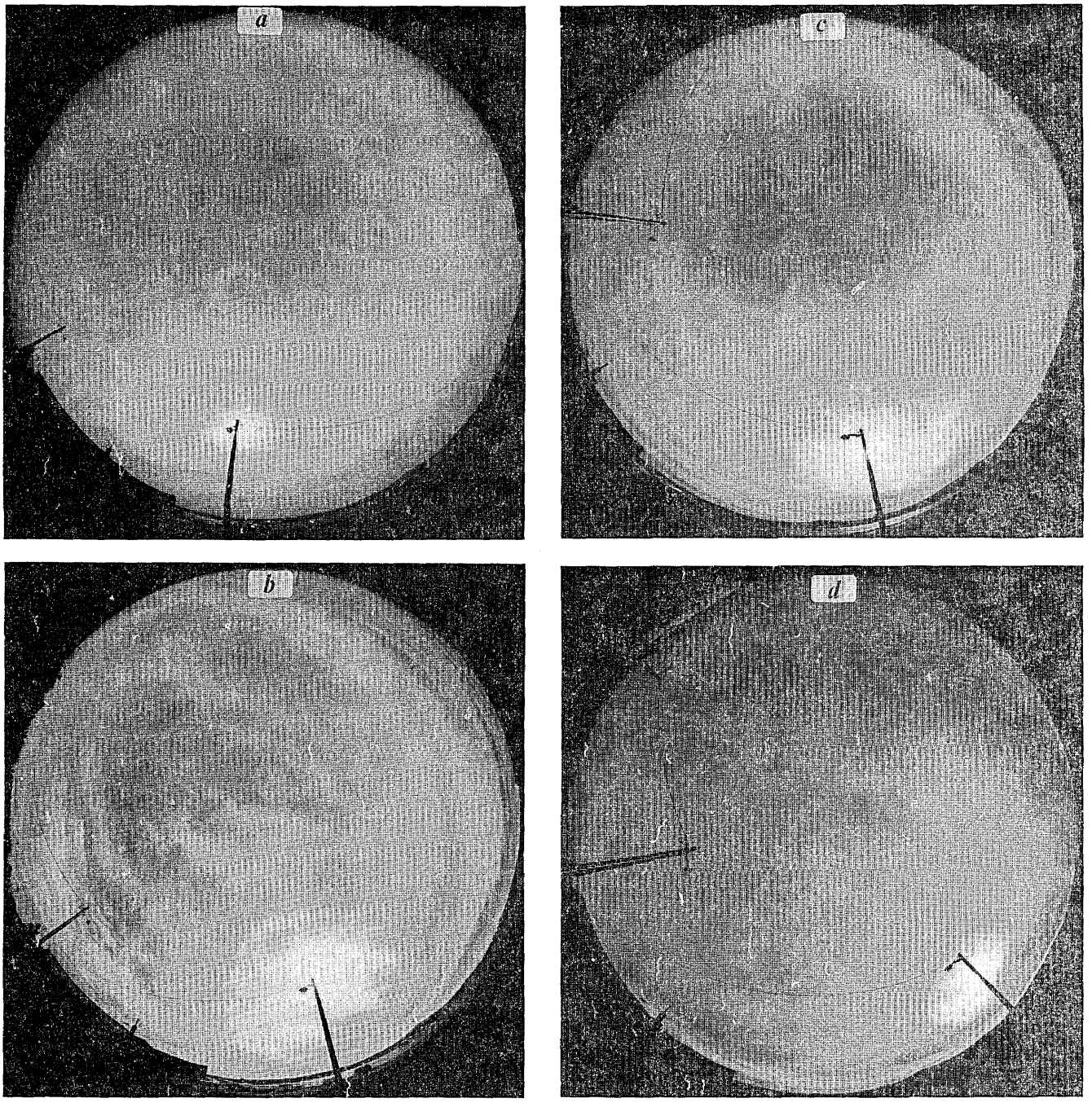

Fig. 1. Examples of 180° fish-eye photographs of cirrus cloud conditions at (a) 1556, 22 October; (b) 1750, 28 October; (c) 1950, 1 November, (d) 2030, 2 November 1986. The 22° halos were often incomplete as a result of multiple scattering and attenuation effects in optically dense particle fallstreaks, especially close to the horizon because of the increased scattering path lengths. The times above are in UTC.

slides that are oil coated (which are kept chilled until examined immediately once on the ground) or that are coated with resins that rapidly evaporate to produce permanent casts of the ice crystals.[2] These instruments can be borne on aircraft or balloons; their heritage can be traced from basic hand-held slide airstream insertion samples collected from World War II military aircraft[3] to later mechanical and decelerator-assisted (to reduce particle impact damage) slide insertion devices,[4] and culminates in continuous aircraft[5] and balloonborne[6] Formvar (i.e., plastic resin) samplers. Although the techniques do not always produce reliable results, in that radial or fragile ice particles may break up and suffer compression on imperfectly prepared substrates during impaction, unique records of the three-dimensional shapes and the internal structures of high-altitude cirrus particles are often obtained.

In this paper we provide numerous photomicrographic examples of the ice particles collected *in situ*

from four cirrus cloud systems that generated 22° halos during periods of coordinated aircraft and ground-based polarization lidar observations. The studies were conducted during the 1986 Project FIRE [First International Satellite Cloud Climatology Program (ISCCP) Regional Experiment] Intensive Field Observation (IFO I) campaign near Wausau, Wis., with the use of the University of Utah mobile polarization lidar (MPL) system and the National Center for Atmospheric Research (NCAR) King Air aircraft, which was equipped with a slide injection device for particle collections. Below, the instrumentation and field project are briefly described, followed by the *in situ* and remote sensing findings for the four cirrus case studies. Although our chief purpose is to describe the cirrus cloud particles associated with 22° halo formation, in view of the scarcity of empirical data from high-altitude cirrus clouds we embellish the photomicrograph collection with more detailed descriptions of the vertical cloud structure and the microphysical content of the cirrus. Then, with the aid of new geometric ray-tracing simulations that describe the angular scattering patterns of more realistic hexagonal ice-crystal models, we interpret the *in situ* data in terms of halo-formation mechanisms in actual cirrus clouds.

2. Field Experiment

During a four-week period in October–November 1986, a field campaign that utilized advanced remote sensing and airborne research instrumentation was conducted over central and southern Wisconsin to characterize the properties of midlatitude cirrus clouds, which were concurrently examined from various satellite platforms.[7] The purpose of this exercise was to enhance our basic knowledge of cirrus clouds, especially with regard to the Project FIRE goal of testing and improving ISCCP cirrus cloud detection and characterization algorithms routed in bispectral satellite radiance observations. One of four ground-based remote sensing sites[8] was located at Wausau in central Wisconsin, which served as a hub for several coordinated University of Utah MPL and aircraft experiments. Four extensive cirrus cloud systems were systematically studied by the lidar and King Air. Each ~2-h aircraft mission consisted of a series of ascending or descending stepped leg profiles along the mean cirrus wind direction and vertical spiral soundings in the immediate vicinity of the ground site. The 20–40-km-long horizontal legs were terminated over Wausau, and the spirals were centered over the site such that the *in situ* data were generally representative of the cirrus cloud conditions probed by the vertically pointed MPL system.

King Air cloud microphysical instrumentation included both two-dimensional crystal (2D-C) and two-dimensional precipitation (2D-P) probes for characterizing the shapes and the sizes of ice crystals, from which composite data algorithms to derive estimates of ice-mass content have been applied.[9] The ice-particle impaction device also deployed collected cirrus ice-crystal samples at frequent intervals by using

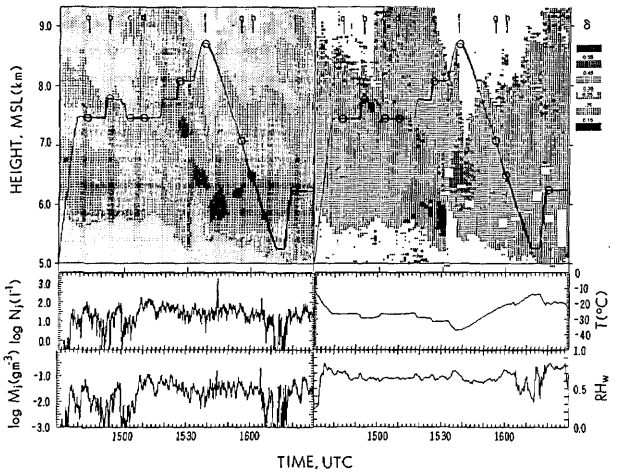

Fig. 2. Combined polarization lidar and *in situ* data displays that cover the indicated 2-h period of the King Air mission on 22 October 1986; they consist of lidar range-normalized returned energy (top left), linear depolarization ratio (top right; see δ value key) HTI displays, and panels of aircraft-derived ice-crystal concentration N_i, ice-mass content M_i, temperature T, and relative humidity RH_w. Curves superimposed on the lidar HTI displays show the supporting aircraft flight track, where the heavy curve segments indicate radial distances from Wausau of <20 km, and the open circles show the times the ice-crystal samples in Fig. 3 (as identified by the letters at top) were collected. Note that the blank regions in the δ display represent the rejection of inaccurate ratios caused by noise in weak signals or off-scale signals in strongly scattering parts of the cirrus cloud.

a relatively simple apparatus that consisted of an aluminum rod with a spring-activated extension at one end. A coated glass slide mounted on that end was exposed to the airstream at velocities of 100–125 ms^{-1} through the aircraft's navigation port. The coatings applied to the slides were most often viscous hexane oils, although other replication materials were tested. Exact exposure times were obtained through an event marker on the inboard end of the rod so that ice-crystal concentration estimates could later be attempted. For the duration of the flight the exposed slides were stored in a dry-ice-cooled container in test tubes that contained a silicone solution that remained fluid at dry-ice temperature and did not absorb water, characteristics essential to ice-crystal preservation. At the end of the flight the samples were transported to a cold room and photographed with an ordinary light microscope.

Because the characteristics of the lidar system as configured during the IFO I campaign have been described previously,[8] only a brief description is given here. The MPL unit utilized a giant-pulsed (1.5-J) ruby (0.694-μm wavelength) laser transmitter and a 25-cm-diameter telescope receiver fitted with dual photomultiplier tube detectors to measure laser backscattering simultaneously in the planes of polarization orthogonal and parallel to the transmitted vertically polarized pulse. From the two digitized (at 7.5-m range resolution) signals, we derive the linear depolarization ratio δ from ratio of the orthogonal to parallel signals after adjusting for differences in the

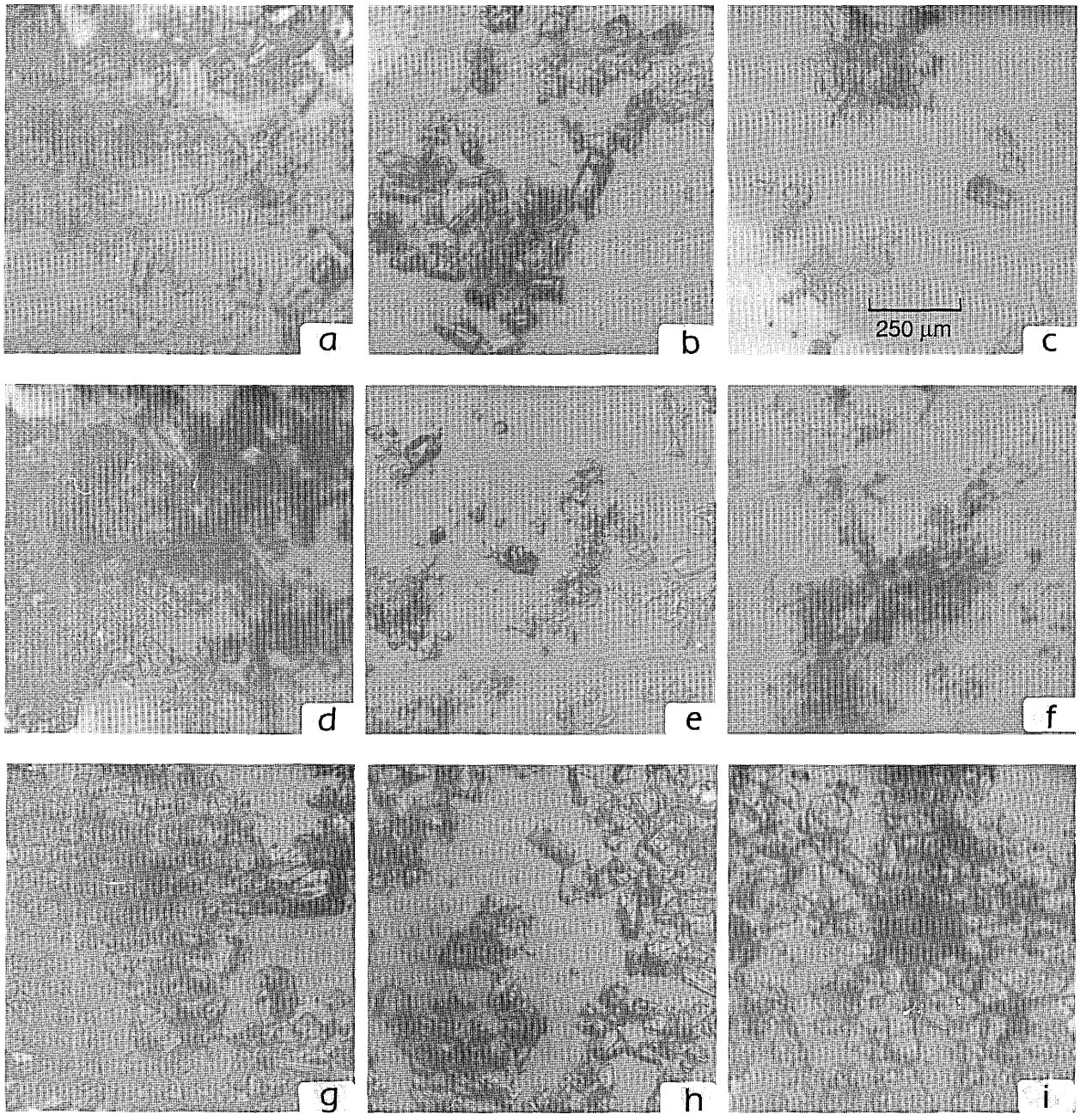

Fig. 3. Representative ice-crystal photomicrographs obtained by impaction on slides (as identified in Fig. 2, top) at the following heights (in kilometers) and temperatures (in degrees centigrade), respectively: a, 7.32, −26.6; b, 7.63, −29.3; c, 7.32, −26.9; d, 7.32, −26.8; e, 7.94, −31.6; f, 8.54, −37.1; g, 6.86, −25.0; h, 6.34, −2..28; i, 6.13, −20.0. Note the 250-μm reference scale in c.

gains of the two channels. The lidar returns were stored on magnetic disk at a rate of 0.5–1 shots per minute. Also collected at ~30-min intervals were 180° black-and-white fish-eye photographs (a red filter was used) showing the appearance of cirrus clouds and the optical displays they generated over the ground site. Examples of the fish-eye photographs for each case study are given in Fig. 1.

In Section 3 comprehensive data displays for the four cirrus cloud case studies are presented. The graphics consist of height-versus-time (HTI) displays of lidar range-normalized returned power (in arbitrary logarithmic units) and linear depolarization ratios over which are superimposed the King Air flight tracks in the vicinity of the ground site, accompanied by *in situ* data panels of combined 2D-C and 2D-P probe-derived ice-crystal concentration N_i and ice-mass content M_i, as well as aircraft-measured temperature T and relative humidity RH_w (with respect to water).

Representative photomicrographs of the ice crystals sampled are given for each case study. Note that all four of these 22° halo-producing studies involved large-scale cirrus cloud systems associated with frontal activity. However, it should be mentioned that these relatively deep cirrus clouds occasion-

ally produced dense fallstreaks and strong optical attenuation that variably obscured portions of the halos.

3. Halo-Producing Cirrus Cloud Case Studies

A. 22 October 1986

The cirrus cloud system studied on this occasion can be characterized as an accumulation of 4–6 km-deep particle fallstreaks. The fallstreaks emanated from cloud-top-generating regions between 10 and 11 km above mean sea level (MSL) (all heights are MSL) and accumulated in the lower cloud region where they often produced strong laser pulse attenuation. During the 2-h period of coordinated King Air studies from ~1430–1630 (all times are UTC), the lidar displays of the aircraft-sampled cloud region(Fig. 2, top) reveal the dominating effects of particle sedimentation from aloft, particularly at ~1540, when a major fallstreak that produced relatively strong ($\delta \gtrsim 0.5$) depolarization (see key at top right) at low levels was probed. According to the superimposed aircraft flight track position and the corresponding microphysical data, the King Air initially measured variable ice-cloud contents (see M_i and N_i plots at lower left) during a rapid ascent of the cirrus, which corresponded to the sampling of the cirrus particle fallstreaks. (The low M_i values just after 1500, e.g., can be seen to correspond to a weak laser-scattering region between fallstreaks.) At 1540 the aircraft climbed to a maximum height of 8.7 km in a region above the optically dense sheared fallstreak (center) that produced range-limiting lidar attenuation effects. The subsequent spiral descent through the cloud layer continued until the aircraft briefly emerged below cloud base at 1615. The lidar linear depolarization display (top right) shows δ values mostly between 0.3 and 0.4, which are rather typical of many cirrus, but also sometimes reveals much lower ratios ($\delta \leq 0.15$, particularly near cloud base at ~1530), as well as $\delta \gtrsim 0.5$ near the bases of the strongly scattering fallstreaks. The low δ values are generally attributable to the effects of horizontally oriented plate crystals (note that the × symbols below the δ-value HTI display represent data collected when the lidar was tipped by more than 2.5° off the zenith direction[10]), whereas the stronger δ values indicate accumulations of complex ice particles, perhaps in the form of aggregates. The fish-eye photograph of Fig. 1(a), taken at 1556, depicts the upper half of a 22° halo whose bottom is obscured by thicker cirrus fallstreaks closer to the horizon.

Photomicrograph examples from the impaction slides that yielded useful data on this mission are given in Fig. 3. (The locations of these samples are identified on the aircraft flight track in Fig. 2, and their heights and temperatures are given in the Fig. 3 caption). Considerable damage to the impacted particles is evident, which indicates the general fragility of ice particles encountered in this case. The easily recognizable elements are hollow bullets that were once members of radial bullet-rosette crystals (Figs. 3a, 3b, and 3d), a hollow column (Fig. 3g, preserved nearly end up), and relatively small solid, or mostly solid, columns (Figs. 3a, 3c, and 3e). Much of the crystal debris can be recognized as fractured hollow columns and bullets (Fig. 3f shows a shattered thin-walled rosette) and parts of hexagonal sector or plate crystals. As the compressed particles in Figs. 3c and 3i resemble compressed radiating groups of sector plates and prismatic crystals, fragile sector-column combinations may also have been common.

B. 28 October 1986

The period of joint ground-based and airborne observations from 1600 to 1800 comprises a portion of the cirrus clouds intensively described in a FIRE IFO I case-study special issue.[11] The cloud system probed over Wausau was again composed of optically dense fallstreaks that caused the 22° halo to become indistinct or incomplete (Fig. 1b). Figure 4 provides the combined lidar and aircraft data in the same form used above. What makes this thick cirrus cloud system unusual, however, is the occasional indication of embedded supercooled liquid-water clouds. These patches of altocumulus clouds are revealed by the $\delta \lesssim 0.15$ values, mostly at altitudes of ~6.7 and 7.8 km; one such patch that produced brilliant iridescent colors can be seen near the center of the Fig. 1b fish-eye photograph. Also in contrast to the above case, *in situ* relative humidity data were periodically near water saturation rather than near ice saturation, which is the minimum needed to maintain pure ice cirrus clouds. Otherwise the lidar depolarization ratios are mostly in the 0.25–0.45 range, which may indicate the presence of horizontally oriented planar ice crystals mixed with other particle types and orientations. An obvious exception to these relatively low δ values occurs at ~1615 at the bottom of a crystal fallstreak, where $\delta \gtrsim 0.55$ values are prevalent.

The somewhat abbreviated King Air mission consisted of a single ascending step-up leg pattern (after 1630) and a rapid spiral descent over Wausau. Considerable variability in cirrus cloud ice content

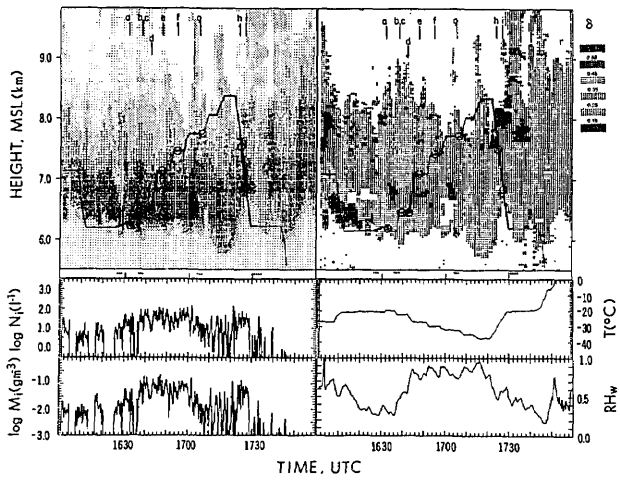

Fig. 4. Combined lidar and aircraft data display as in Fig. 2, but showing the results of the aircraft mission at the indicated times on 28 October 1986.

(Fig. 4, bottom left) is associated with the aircraft fallstreak penetrations, and M_i and N_i tend to increase with decreasing altitude. (Note in particular the vigorous fallstreak that descended, at ~1715, to an altitude of 5.7 km, which is well below the usual cloud base.) The corresponding ice-crystal photomicrograph collection given in Figs. 5a–5i shows that hollow bullet-rosette crystals and their derivatives, following impaction at the 100–125-ms^{-1} airspeeds, are clearly dominant. Quite thin-walled bullets are particularly evident in Figs. 5a, 5d, and 5g, shattered hollow columns are evident in Fig. 5b, and mostly solid bullet remnants are evident in Figs. 5e and 5i. In addition, shattered sector-column and simple plate-crystal remnants are depicted in Fig. 5f. Also note the rounded crystal forms in Fig. 5a, which were collected near the cloud base in quite dry air.

C. 1 November 1986

This third cirrus cloud system was also dominated by the action of deep, sheared ice-particle fallstreaks, which created a strongly scattering cloud base region between 5 and 6 km (Fig. 6). The occurrence of a complete 22° halo was accordingly sporadic, but an enhancement of the upper-tangent arc region was often apparent (Fig. 1c). The King Air performed a

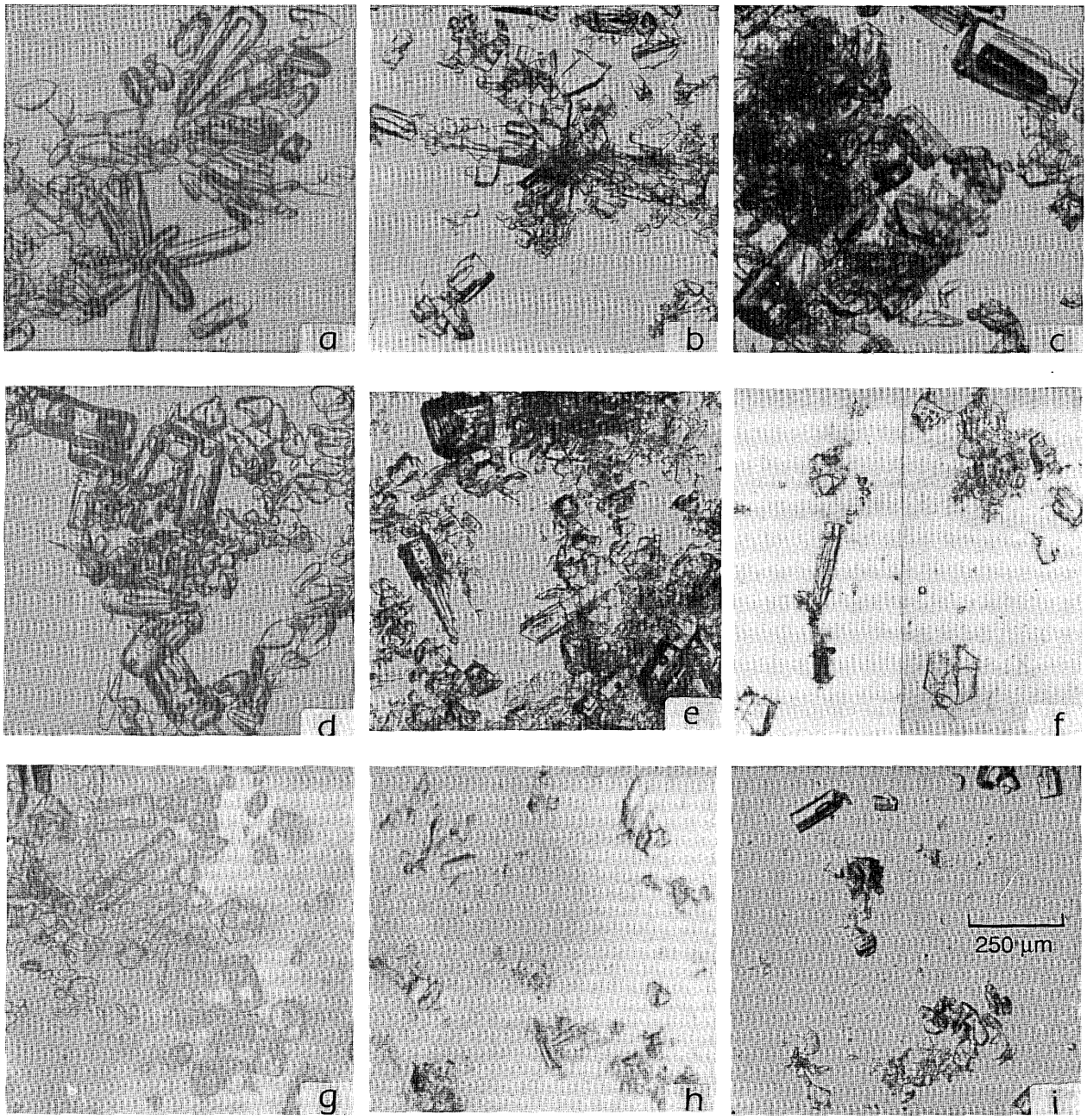

Fig. 5. Ice-crystal photomicrographs obtained (see Fig. 4, top) at the following heights (in kilometers) and temperatures (in degrees centigrade), respectively: a, 6.13, −20.0; b, c, 6.38, −22.2; d, 6.38, −22.2; e, 7.01, −26.9; f, 7.34, −29.8; g, 7.62, −32.2; h, 7.26, −29.2; i, 6.72, −25.2. A 250-μm scale is provided in i.

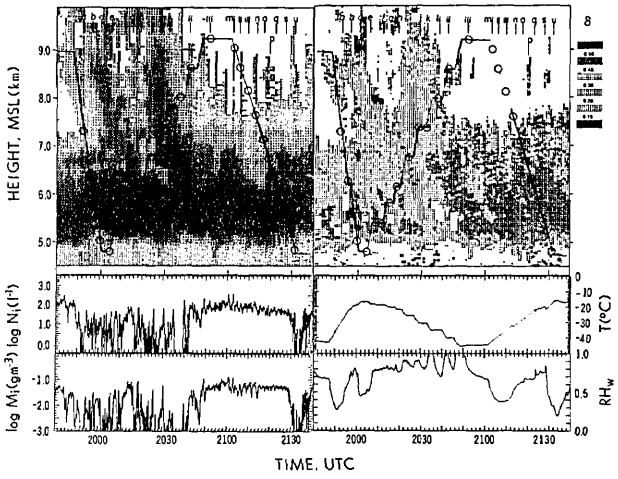

Fig. 6. Combined lidar and aircraft data display as in Fig. 2, but showing the results of the aircraft mission at the indicated times on 1 November 1986.

mission that consisted of a rapid descent, a stepped ascent, and a spiral descent through the cirrus clouds above Wausau (see Fig. 6, top). Variability in ice content that is attributable to aircraft fallstreak penetrations is initially apparent, but during the final descent M_i and N_i are relatively high and constant, which indicates that the Eulerian spiral remained within the domain of a fallstreak during descent. Laser depolarization was relatively strong (~ 0.5) in the cloud region accessible to lidar probing (because of attenuation) during the spiral descent of the aircraft, as it also was at times near the lower boundaries of the fallstreaks. Occasional evidence for horizontally oriented planar ice crystals is present.

The ice crystals photomicrographed on this occasion are quite well preserved and varied, as can be seen from Fig. 7. Although hollow columns that display intricate internal structures dominate, also present are thick plates (Figs. 7a, 7c, and 7e), simple plates (Fig. 7g), bullet rosettes (Fig. 7n), and a plate-capped column crystal that fortuitously survived impaction (Fig. 7k). In addition, the remnants of radial-sector or column-sector assemblages are evident in Figs. 7g, 7h, 7q, and 7t, which are perhaps also responsible for the shattered debris obtained near cloud top (Figs. 7l and 7m). Unusual ice-crystal replicas include the seemingly identical, paired-column crystals[12] in Fig. 7b, and the spatial prism growths in Figs. 7f and 7h. Finally, ice crystals collected near the cirrus cloud base (Figs. 7d, 7e, 7s, and 7t), where rapid particle evaporation was occurring in dry air, displayed rounded crystal forms that affected the laser-scattering behavior of these particles. Ice-crystal faces that lack sharp definition (because of evaporation) relative to the incident wavelength often generate decreased δ values at the lower boundary of cirrus clouds, as is apparent from Fig. 6.

D. 2 November 1986

The fish-eye photograph from 2030 in Fig. 1d shows an incomplete 22° halo, which was typical of the conditions associated with the cirrus cloud system studied on the morning of 2 November. The King Air, over Wausau, performed a mission consisting of a step-up leg pattern bracketed by two spiral descents (Fig. 8, top). Although the cloud microphysical data record is incomplete, the variability in ice content is again in general agreement with the presence of the lidar-detected deep-precipitation fallstreaks, which at times (especially at ~ 2050) produced strong optical attenuation. Lidar depolarization was typically in the 0.4–0.5 range, although much lower δ values were measured at ~ 2115 at an altitude of 6.7 km from an embedded supercooled (~ -31 °C) altocumulus cloud. (Note that the $\delta < 0.15$ values below the cloud base and between the lower portions of the fallstreaks from 2100 to 2120 represent the effects of a mixture of molecular and quite weak cirrus cloud returns.)

Figure 9 reveals that this deep cirrus cloud comprised chiefly bullet-rosette crystals, which displayed considerable hollowness. There is again evidence, however, for sector-column combinations (Figs. 9d and 9p), and in Fig. 9k a large (~ 800-μm-long) shattered hollow column crystal is shown. Columns that display only a small amount of internal structure are also preserved (Figs. 9c and 9n), but obviously they constitute a relatively minor component of the ice crystals sampled.

4. Halo Ray-Tracing Considerations

In recent years a significant advancement in our ability to treat the light-scattering properties of realistically shaped ice crystals has resulted from the (albeit computer-intensive) programs based on geometric optics ray-tracing principles.[13,14] These numerical experiments have utilized models that display the widely accepted hexagonal symmetry of ice crystals through a range of realistic axial ratios, including both solid column and plate structures, but in view of *in situ* evidence that indicates considerably more complicated cirrus cloud particle structures, it can be questioned whether such simple models are appropriate. Fortunately ray-tracing predictions that involve the first step toward more realistic ice-crystal models are now available, as we show in Figs. 10 and 11.

As the solid hexagonal column model has frequently been used to simulate cirrus cloud halo properties,[15,16] we present for comparison ray-tracing phase functions for randomly oriented solid columns, which are denoted as the solid-dashed curves in Figs. 10 and 11. Such idealistic particles generate a quite well-defined 22° halo and, to a lesser but still noticeable extent, a 46° halo. However, it is obvious that if one treats simple hollow-ended column structures (Fig. 10), then the inner edge of the 22° halo becomes considerably less distinct, whereas the 46° halo vanishes. (Previously published 46° halo simulations relied on solid column-crystal end-on refractions.[15]) Column ice-crystal backscattering is also significantly diminished by the hollow ends.

A comparison of ray-tracing phase functions for randomly oriented solid columns and a solid (i.e.,

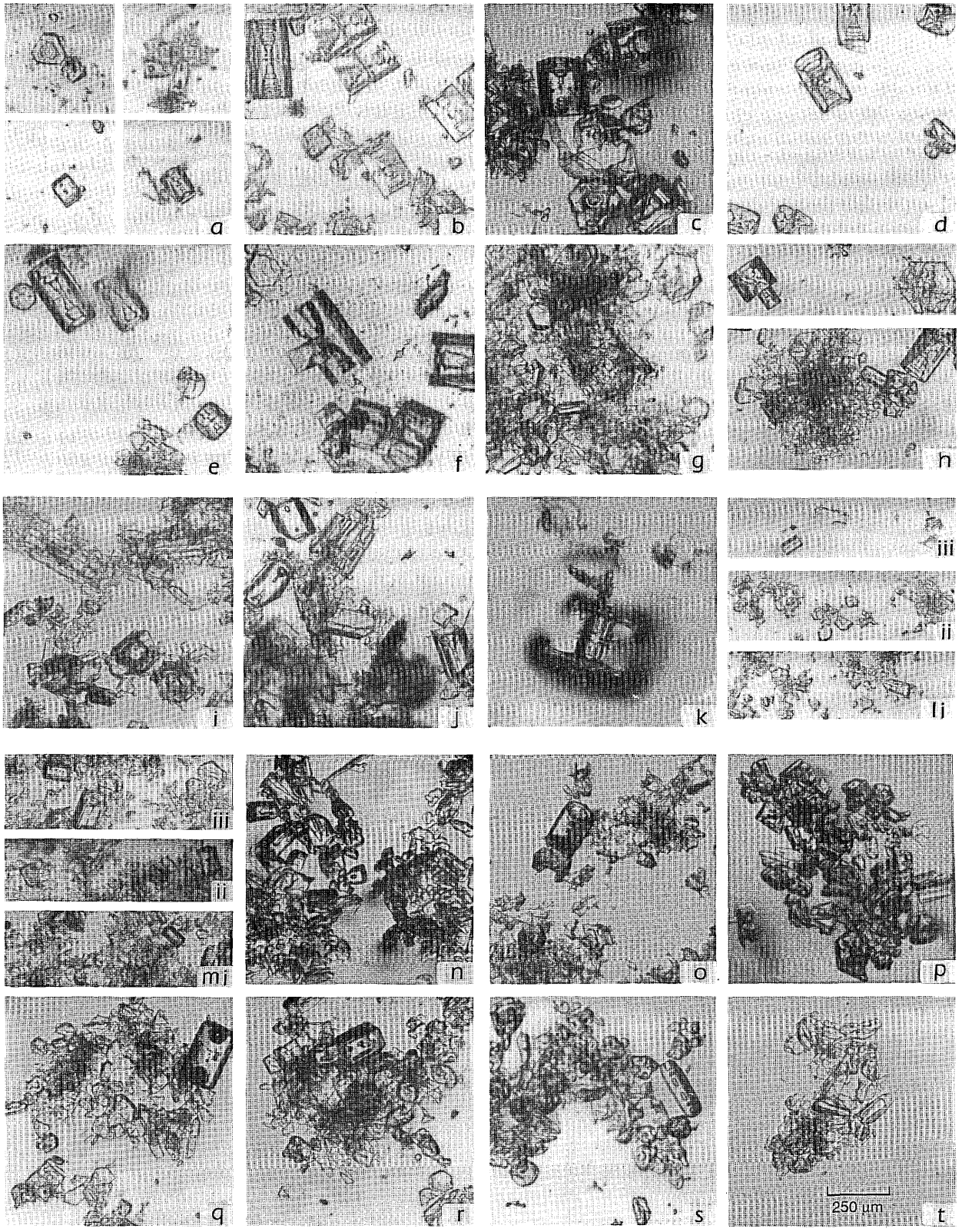

Fig. 7. Ice crystal photomicrograph obtained (see Fig. 6, top) at the following heights (in kilometers) and temperatures (in degrees centigrade), respectively: a, 7.15, −29.3; b, 6.15, −21.9; c, 5.58, −19.3; d, 4.84, −17.6; e, 4.78, −17.3; f, 5.34, −18.8; g, 5.76, −20.4; h, 6.10, −21.6; i, 6.70, −25.7; j, 7.32, −30.6; k, 7.31, −30.6; li, 7.91, −35.1; lii, 8.54, −40.4; liii, 9..15, −44.9; mi, 8.88, −42.5; mii, 8.49, −39.1; miii, 8.03, −35.7; n, 7.53, −32.2; o, 7.00, −28.3; p, 6.60, −25.4; q, 6.19, −22.6; r, 5.49, −19.7; s, 5.17, −19.9; t, 4.75, −16.1. The 250-μm scale in t applies to all particles.

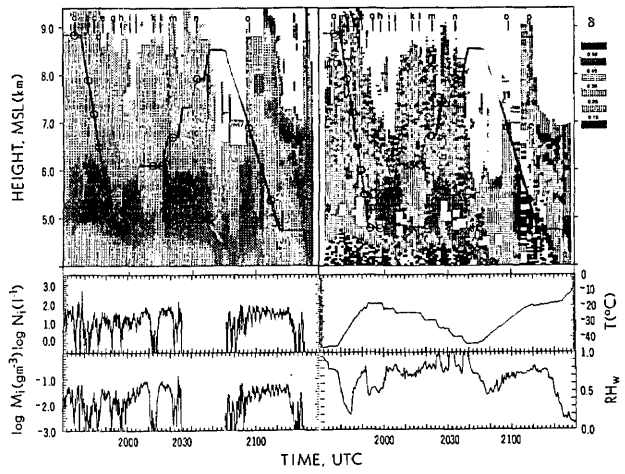

Fig. 8. Combined lidar and aircraft data display as in Fig. 2, but showing the results of the aircraft mission at the indicated times on 2 November 1986. Note that 2D-C and 2D-P probe data are missing from 2025 to 2046 and after 2123.

idealistic) bullet-rosette ice-crystal model is given in Fig. 11 (see figure caption for details). In this case, because of the unreasonably pristine nature of the pointed hexagonal bullet tips (compared with the previous photomicrographs), a ~8° halo emerges. However, with more irregular bullet tips the scattered intensity to the left of the 22° halo could still be expected to fill in without the formation of the (rarely observed) 8° halo. Although the 46° halo and backscattering are diminished, the use of hollow-ended bullets would no doubt have produced more dramatic effects similar to those in Fig. 10 for hollow-ended columns. Also note that bullet-rosette sidescattering increases markedly as a result of the complicated ray-tracing patterns induced by neighboring ice-crystal elements.

5. Conclusions

These detailed remote and *in situ* observations of four 22° halo-producing cirrus cloud systems provide a unique data set that can be applied to explain the occurrence of the common halo and, inversely, the nonoccurrence of optical displays in many, if not most, cirrus clouds. It is apparent that in contrast to the traditional ice-particle model postulated by 22° halo theorists, i.e., the randomly oriented solid hexagonal crystal, the actual structures of halo-producing cirrus ice crystals are far more complex. It can generally be said that the intricacy of cirrus ice-crystal internal and radial structures violates the simple assumptions usually applied to modeling the scattering behavior of these high clouds. Solid or mostly solid ice crystals, which could be expected to be comparatively well represented in the impacted particle sample, are obviously uncommon. The major distinctions between the traditionally modeled and the cirrus ice-crystal shapes obviously lie in the internal hollow structures and radial forms of the cloud particles. (Column and bullet-rosette crystals are frequently so thin walled as to shatter on collection.) However, this finding should not be considered as groundbreaking, as it has been previously pointed out from aircraft observations that cirrus clouds composed of hollow or radial crystals are capable of generating halos.[3,17]

How this diversity in cirrus ice-crystal shape relates to visible (0.69-μm) lidar linear depolarization is difficult to judge because the sporadic impaction samples were not obtained directly over the ground site: a more continuous impaction device and better aircraft navigation (both of which are now available) would have been better suited for this purpose. Nonetheless, we can attempt to make generalized intercomparisons between the dominant ice-crystal habits measured *in situ* and the distributed fields of δ values when the aircraft made close approaches. On 1 and 2 November, for example, relatively strong lidar depolarization (0.45–0.55) was widespread, and, as expected from basic scattering principles,[10] the corresponding dominant crystal types were complexly shaped. On 2 November bullet rosettes and their aggregates (Figs. 9e–9i) appeared responsible for δ values of as high as ~0.6 in the lower cirrus, whereas on 1 November it was highly structured hollow columns (Figs. 7b–7f) and sector-column radial crystals (Figs. 7p–7s) that were indicated to have produced strong depolarization. The cirrus clouds on 22 and 28 October consistently produced lower δ values. Widespread cloud regions that displayed 0.25–0.35 and 0.35–0.45 δ values were probed by the aircraft; we assume that these values represent a mixture of prismatic crystals and horizontally oriented plate or capped-column crystals, which are chiefly preserved in the *in situ* samples as shattered bits of sectors (Figs. 3 and 5). Oriented plate-crystal lidar-scattering anisotropy was occasionally noted to be present in both these cases, presumably from cloud regions that were dominated by plate specular reflections. Finally, the tendency for δ values to decrease significantly at the cirrus cloud base and perhaps in subsaturated regions within the clouds has been linked to evaporating crystals that lose their hexagonal scattering faces. Although previous theoretical research has shown lidar depolarization to be influenced by the basic hexagonal ice-crystal shape (i.e., axial ratio) and orientation,[13] it is clear that the shape complexities displayed by cirrus ice crystals need to be simulated more accurately to improve the interpretation and the utility of polarization lidar returns.

The geometric optics ray-tracing phase-function predictions given here for ice-crystal shapes that begin to approach the complexity of the particles captured *in situ* are noteworthy, despite their still simplistic nature. Through the inclusion of hollow-ended column and radial-bullet-scattering effects, a number of interesting angular scattering features have been revealed. In agreement with observations of many halos, the distinctiveness of the inner edge of the 22° halo, as well as the entire 46° halo, declines noticeably. Backscattering is also diminished, whereas sidescattering in the case of bullet rosettes is

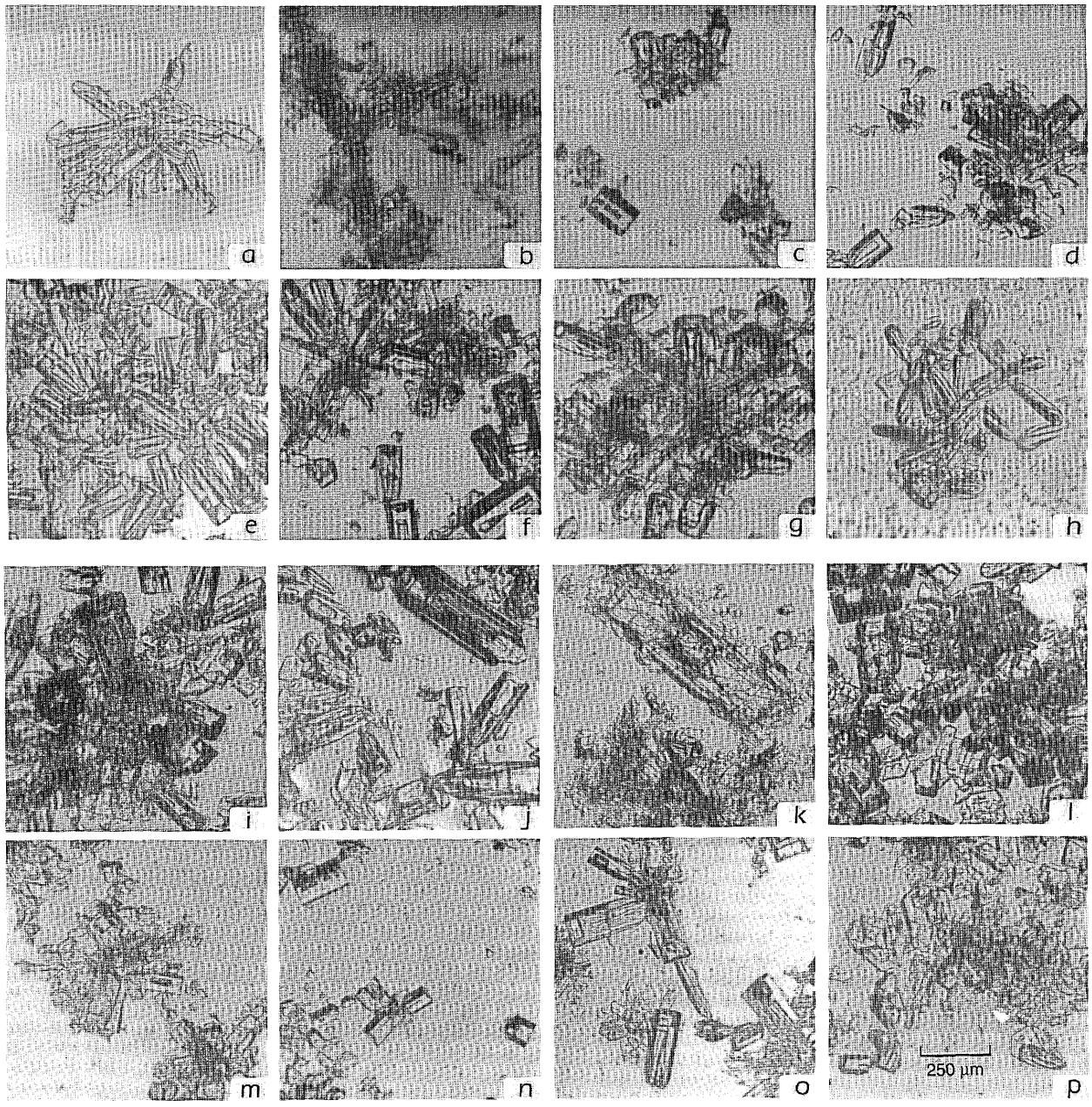

Fig. 9. Ice-crystal photomicrographs obtained (see Fig. 8, top) at the following heights (in kilometers) and temperatures (in degrees centigrade), respectively: a, 8.84, −46.3; b, 7.70, −36.7; c, 7.12, −31.9; d, 6.34, −26.5; e, 5.80, −23.8; f, 5.27, −21.9; g, 4.77, −18.9; h, 4.76, −18.5; i, 5.49, −21.8; j, 5.71, −22.5; k, 6.10, −24.5; l, 6.10, −24.8; m, 6.70, −29.3; n, 7.93, −39.6; o, 6.79, −30.9; p, 5.30, −20.2. Scale is provided in p.

significantly enhanced. These findings not only have implications for halo formation (e.g., in explaining why the 46° halo is rarely seen), but may also improve our understanding of satellite-based radiance methods for inferring cirrus cloud properties. In this regard we point out that the increase in cirrus cloud sidescattering predicted for radial ice crystals helps to alleviate the necessity for evoking the presence of numerous small ice particles in cirrus.[1]

Finally, the question of why halos in cirrus clouds are not more commonly observed can be addressed. According to previous ray-tracing simulations, the 22° and the 46° halos should be prominent features as long as simple hexagonal ice crystals, somewhat larger than the wavelength,[18] are (mostly) randomly oriented.[19,20] In contrast, in cirrus clouds the complexity and the diversity of particle shape interferes with halo formation, unless conditions are appropriate for the generation of at least partially solid crystals in sufficient numbers. As an examination of the more memorable historic halo displays reveals an association with low-altitude winter or polar ice-crystal clouds, rather than typical cirrus, it is apparent that cirrus particle growth processes often result in unsuitable crystal habits. Not only does the *in situ* evidence indicate that typical cirrus particles are

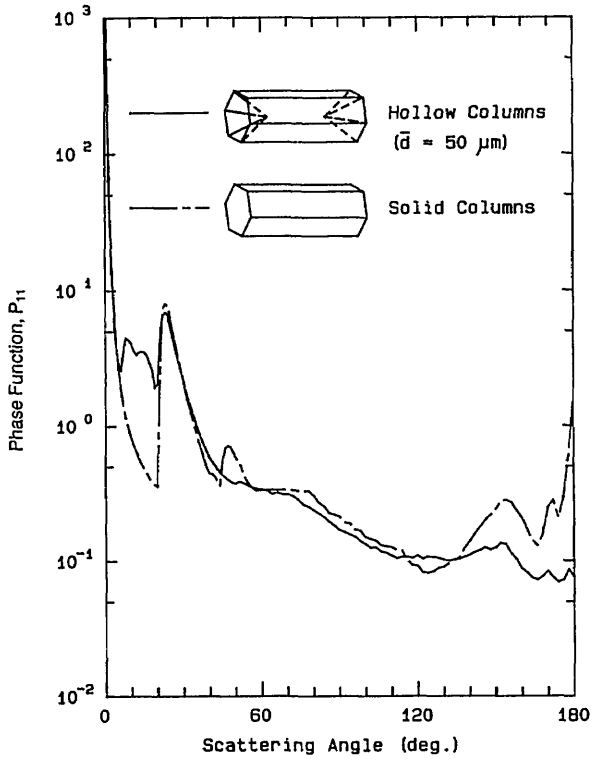

Fig. 10. Comparison of ray-tracing-predicted phase functions P_{11} for randomly oriented hexagonal solid and hollow-ended columns (see inserts) computed for a 0.55-μm wavelength. Both column models are 200 μm in length and 80 μm in maximum width: the depths d of the hollow ends are 50 μm.

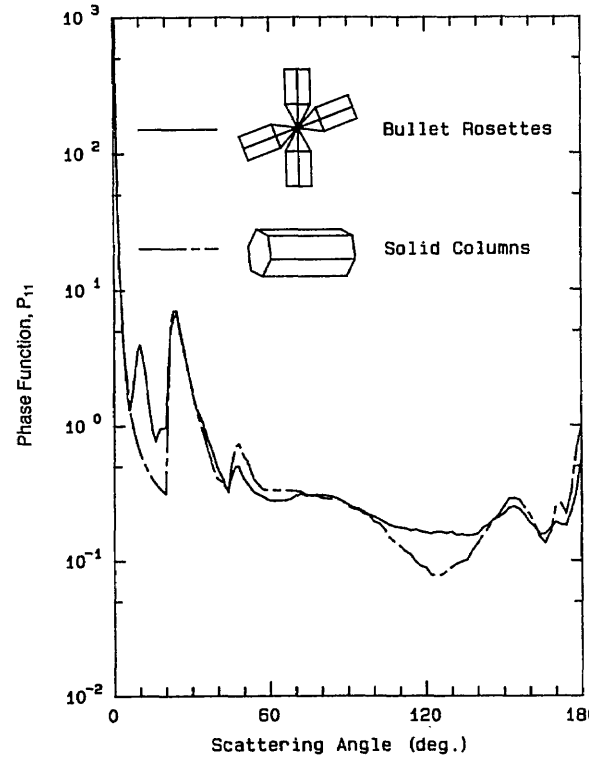

Fig. 11. Comparison of ray-tracing-predicted phase functions, again at a 0.55-μm wavelength between randomly oriented solid columns and bullet rosettes (see inserts). Each of the four solid bullets (aligned radially in the same plane) is 60 μm in width and 240 μm in total length, inclusive of the 48-μm-long pointd bullet tip. The 200-μm length and 100-μm width of the columns are based on a projected area that is equal to that of the randomly oriented bullet rosettes.

too hollow or complex to produce vivid halos, but multiple scattering in optically thick cirrus and the evaporaton of cirrus particles, an integral part of the cirrus cloud growth–maintenance process,[8] detracts from halo formation. As all cirrus clouds are precipitating and may not be actively renewing themselves locally, decaying cirrus may not be capable of producing halos as a result of the rounded crystal forms produced during descent through subsaturated air.

We conclude that, to satisfy the requirement for randomly oriented hexagonal particles, refracted ray paths through the solid portions of bullet crystals in radial rosettes are capable of generating (rather unexceptional) 22° halo displays. Mostly solid particles must comprise a sufficient proportion of the cirrus content, however, to ensure that near forward scattering from more complex internal reflections and refractions does not dominate in the halo region. Similarly, during the 1 November 1986 case study, an often indistinct upper-tangent arc to the 22° halo was observed in association with partially solid column crystals large enough to maintain horizontal orientations. Exceptionally vivid halo formation in cirrus clouds is thus reliant on the generation of solid ice crystals and the still largely unknown cloud microphysical conditions responsible for their growth.

Support for the University of Utah participation in the FIRE IFO project and partial support for the NCAR King Air was provided by National Science Foundation grant ATM-8513975. Recent research at the University of Utah has been funded by National Science Foundation grant ATM-8914348 and NASA grant NAG-1-868 for cirrus data analysis and by National Science Foundation grant ATM-9024217 for scattering theory development. King Air data analysis at NCAR was funded under NASA contract L98110B. The National Center for Atmospheric Research research is sponsored by the National Science Foundation.

References and Notes

1. K. Sassen, A. J. Heymsfield, and D. O'C. Starr, "Is there a cirrus small particle radiative anomaly?" in *Preprints of the Seventh Conference on Atmospheric Radiation* (American Meteorological Society, Boston, Mass., 1990), pp. J91–J95.
2. V. J. Schaefer, "A method for making snowflake replicas," Science **93,** 239–240 (1941).
3. H. K. Weickman, "Die Eisphase in der Atmosphär," Lib. Trans. **273** (Royal Aircraft Establishment, Farnsborough, UK, 1947).
4. A. J. Heymsfield and R. G. Knollenberg, "Properties of cirrus generating cells," J. Atmos. Sci. **29,** 1358–1366 (1972).
5. P. A. Spyers-Duran and R. R. Braham, Jr., "An airborne continuous cloud particle replicator," J. Appl. Meteorol. **6,** 1108–1113 (1967).
6. C. Magono and S. Tazawa, "Design of snow crystal sondes," J. Atmos. Sci. **23,** 618–625 (1966).

7. D. O'C. Starr, "A cirrus-cloud experiment: Intensive field observations planned for FIRE," Bull. Am. Meteorol. Soc. **68,** 119–124 (1987).
8. K. Sassen, C. J. Grund, J. D. Spinhirne, M. Hardesty, and J. M. Alvarez, "The 27–28 October 1986 FIRE IFO cirrus case study: a five lidar overview of cloud structure and evolution," Mon. Wea. Rev. **118,** 2288–2311 (1990).
9. A. J. Heymsfield, K. M. Miller, and J. D. Spinhirne, "The 27–28 October FIRE IFO cirrus case study: cloud microstructure," Mon. Weather Rev. **118,** 2313–2328 (1990).
10. K. Sassen, "The polarization lidar technique for cloud research: a review and current assessment," Bull. Am. Meteorol. Soc. **72,** 1848–1866 (1991).
11. The November 1990 (Vol. 118) issue of the *Monthly Weather Review* compiles a number of related articles from this cirrus cloud case study.
12. N. C. Knight, "No two alike," Bull. Am. Meteorol. Soc. **69,** 496 (1988).
13. Y. Takano and K. N. Liou, "Solar radiative transfer in cirrus cloud. Part I: single-scattering and optical properties of hexagonal ice crystals," J. Atmos. Sci. **46,** 3–19 (1989).
14. K. N. Liou and Y. Takano, "Light scattering by nonspherical particles: remote sensing and climatic implications," Atmos. Res. (to be published).
15. R. Greenler, *Rainbows, Halos, and Glories* (Cambridge U. Press, Cambridge, 1980).
16. R. A. R. Tricker, *Ice Crystal Haloes* (Optical Society of America, Washington, D.C., 1979).
17. M. Glass and D. J. Varley, "Observations of cirrus particle characteristics occurring with halos," in *Preprints of the Conference on Cloud Physics and Atmospheric Electricity* (American Meteorological Society, Boston, Mass., 1978), pp. 126–128.
18. According to the laboratory studies reported in K. Sassen and K. N. Liou, "Scattering of polarized laser light by water droplet, mixed phase and ice clouds. Part I: Angular scattering patterns," J. Atmos. Sci. **36,** 838–851 (1979), minimum ice-crystal dimensions of ~ 25 μm are needed for generating halos.
19. K. Sassen, "Remote sensing of planar ice crystal fall attitudes," J. Meteorol. Soc. Jpn. **58,** 422–429 (1980).
20. K. Sassen, "Polarization and Brewster angle properties of light pillars," J. Opt. Soc. Am. A **4,** 570–580 (1987).